Supplementary information

Effect of Liquid-Sheet Jet Flow Velocity on Lithium Detection Sensitivity in Aqueous Solutions via Laser-Induced Breakdown Spectroscopy

Yuwei Tian[a], Zhixing Gao[a*], Yuanhang Wang[a*], Zhao Wang[a], Zhenlin Hu[b], Linyuan Cao[c], and Hongzhi Cheng[a]

I. The stability of the laser energy.

Table S1 The stability of laser energy test results

Head	PEBF-DFH-C		
Range	200 mJ	**Laser**	1064
Readings	100	**Average**	55.0 mJ
Minimum	54.3 mJ	**Std Dev**	0.249 mJ
Maximum	55.6 mJ		

The measurements were conducted under standard laboratory conditions, specifically at a temperature of 25° C and a humidity level of 40%.

II. Optimization of laser focusing position and flat nozzles.

The laser interaction point was positioned sufficiently close to the nozzle exit to minimize variations in liquid thickness caused by flow, which can affect signal intensity. To verify the stability of liquid thickness at this position, the liquid-sheet jet was recorded using a high-resolution intensified IsCMOS camera (ZWTP428YD, Beijing Zhanwang Youye Technology Co., Ltd.) at a liquid velocity of 2.9 m/s. The image intensifier delay was set to 245 μs, and the integration time was 100 μs and 100 ms. The results, presented in Fig.S1, indicate that thickness variations are negligible when the laser interacts at a distance of 1 mm from the nozzle. Additionally, it was necessary to ensure that the generated plasma did not extend to the nozzle exit to prevent potential damage. Therefore, the laser could not be positioned too close to the nozzle. The plasma plume diameter was typically found to be about 0.7–1.0 mm, indicating that a distance of 1 mm between the laser focus and the nozzle exit is appropriate.

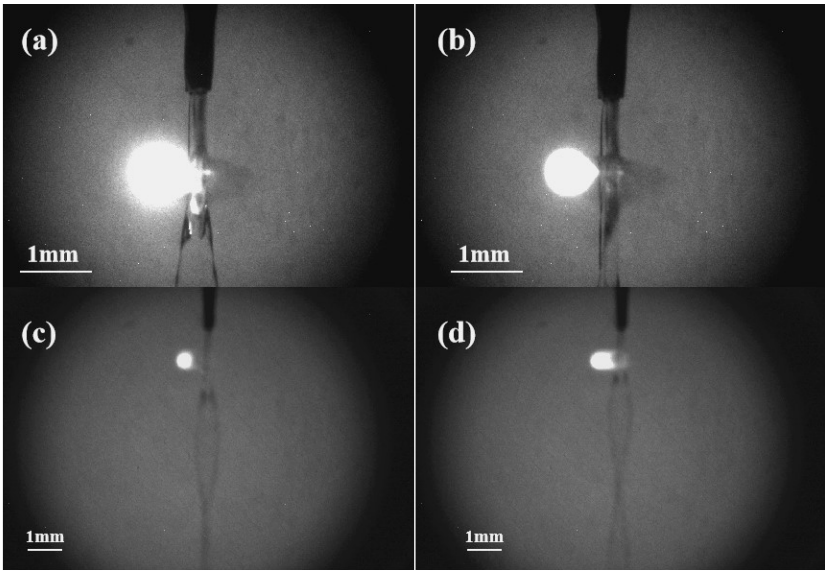

Fig. S1. High-Resolution Imaging of Liquid Thickness Stability in a Liquid-Sheet Jet at 1 mm Laser Interaction Point with Integration Times of (a)(b) 100 μs and (c)(d) 100 ms.

By adjusting the pump rotation speed to ensure that liquid samples were jetted at the same flow velocity through flat nozzles of varying specifications, the spectral intensity and signal-to-noise ratio (SNR) at Li I 670.78 nm were compared. A flow velocity of 2.9 m/s was selected for the optimization process, as this velocity just allowed for the formation of a continuous liquid sheet. The optimization results are presented in Fig. S2, where each data point represents the average of 15 individual measurements, with error bars indicating the standard deviations. Detailed specifications of the flat nozzles used in the optimization are provided in Table S2.

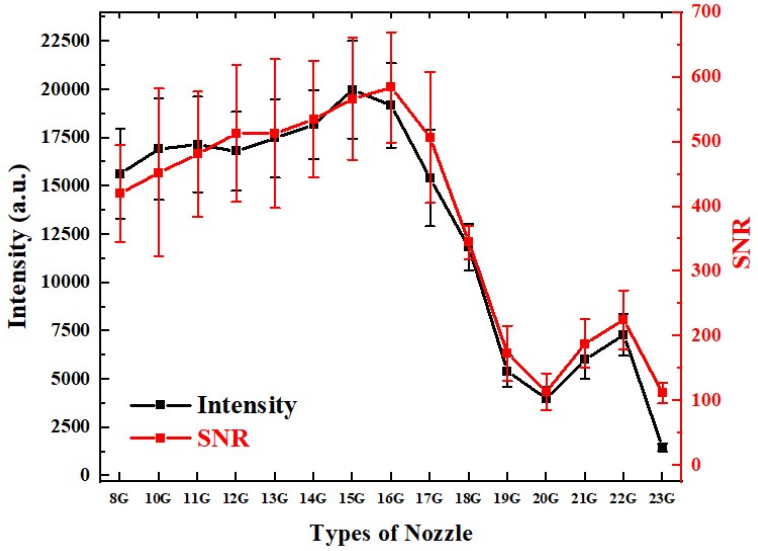

Fig. S2. The spectral intensities and SNRs with different flat nozzle specifications for Li I 670.78nm.

Table S2 The parameters of different specifications of flat nozzles

	specification	Flat mouth wide (mm)	Flat mouth thick (mm)	Revolution (r/min)	Velocity (m/s)
	8G	5.86	0.42	112.6	2.9
	10G	5.05	0.45	103.9	2.9

	11G	4.27	0.44	86.1	2.9
	12G	3.97	0.43	78.3	2.9
	13G	3.35	0.42	64.6	2.9
	14G	2.89	0.41	54.1	2.9
	15G	2.46	0.43	48.5	2.9
	16G	2.15	0.43	42.1	2.9
	17G	1.96	0.37	33.4	2.9
	18G	1.65	0.36	27.0	2.9
	19G	1.42	0.30	15.1	2.9
	20G	1.19	0.24	13.3	2.9
	21G	0.98	0.29	12.8	2.9
	22G	0.92	0.19	7.8	2.9
	23G	0.82	0.17	6.4	2.9

III. The relationship between the pump revolution and the flow velocity.

Table S3 The relationship between the pump revolutions and the liquid flow velocity

Revolution (r/min)	Flow velocity (m/s)
40	2.90
50	3.63
60	4.38
75	5.14
90	5.89
100	6.58
110	7.33
120	8.08
130	8.84
140	9.52
150	10.28
160	11.03
170	11.78
180	12.47
190	13.22
200	13.98
210	14.73

IV. Schematic diagram of the capillary effect.

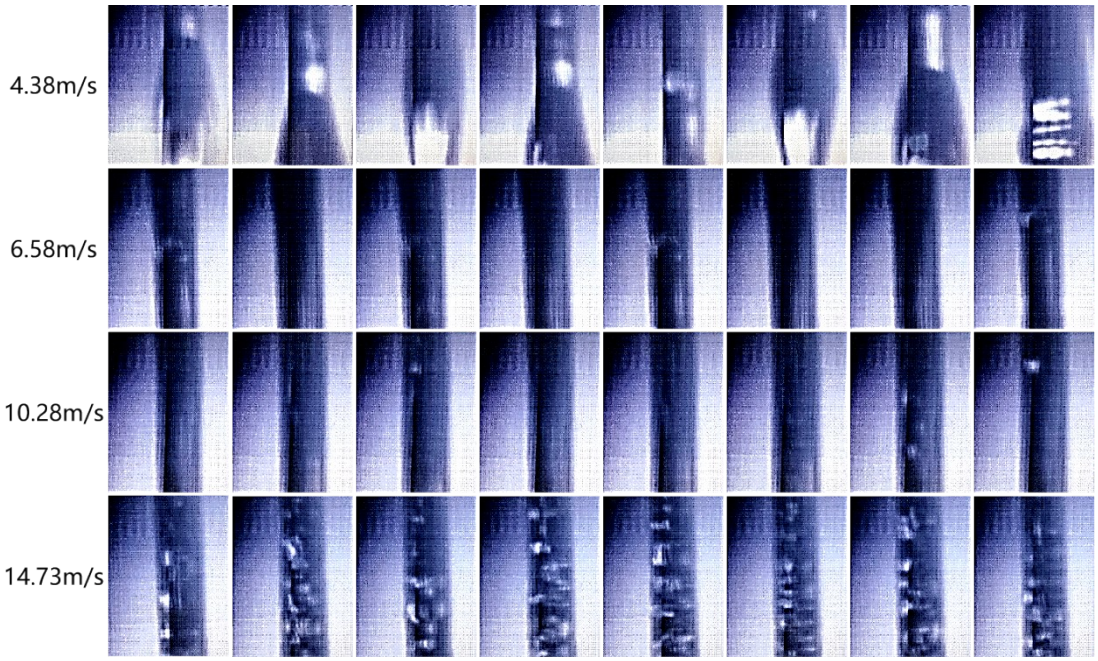

Fig. S3. The dynamic images of liquid flow sheet at different flow velocity.

To investigate the mechanism how liquid flow velocity affects LIBS signals, this study conducted a detailed observation of liquid flow dynamics under different flow velocity and captured dynamic images. Fig. S3 presents the narrow-face dynamic images of liquid flow at four different velocity. The observations indicate that at lower flow velocity, the liquid flow exhibited significant instability, accompanied by noticeable fluctuations. At higher flow velocity, a large amount of air bubbles mixed into the liquid flow, which is speculated to the increased Reynolds number caused by higher velocity, leading to turbulence.

The Reynolds number (Re) is a dimensionless number used to predict the flow state of a fluid, typically representing the ratio of inertial forces to viscous forces in the fluid. The formula for calculating the Re is as follows:

$$Re = \frac{\rho v L}{\mu} = \frac{v L}{\nu} \tag{1}$$

where, ρ is the fluid density, v is the characteristic velocity of the fluid, L is the characteristic length, usually the hydraulic diameter of the flow channel or the characteristic size of the object, μ is the dynamic viscosity of the fluid, and ν is the kinematic viscosity of the fluid, which equals the dynamic viscosity divided by the density.

By analyzing the Re to determine the flow regime, it helps to judge whether the flow is laminar or turbulent. If $Re < 2000$, the flow is usually laminar, with fluid particles moving along parallel paths and the flow being smooth; if $2000 < Re < 4000$, the flow state may transition

from laminar to turbulent; if $Re > 4000$, the flow is usually turbulent, with fluid particles moving along complex paths and the flow being chaotic.

V. Calculation of the plasma electron density and excitation temperature.

This study calculates the electron density using the Stark broadening of the H I 656.28 nm spectral line. The calculation formula is as follows:

$$n_e = 10^{17}\left(\frac{\Delta\lambda_{1/2}}{0.549}\right)^{1.4713} \tag{2}$$

where, $^{\Delta\lambda_{1/2}}$ represents the full width at half maximum (FWHM) of the spectral line. Since the Stark broadening of the spectral line follows a Lorentzian profile, the spectral line can be fitted using a Lorentzian curve to obtain $^{\Delta\lambda_{1/2}}$, which is then used to calculate the electron density.

The excitation temperature is determined using the Boltzmann plot method:

$$y = mx + q_s \tag{3}$$

where, $y = ln\frac{I_{ki}}{A_{ki}g_k}$, $x = E_k$, $m = -\frac{1}{K_B T}$, $q_s = ln\frac{FC_s}{U_S(T)}$. I_{ki} is the integrated intensity, expressed in photons·s/cm^3, typically averaged over multiple measurements. F is an experimental parameter related to the optical efficiency of the collection system, as well as the density and volume of the plasma. C_s is the number density of element particles s (particle/cm^{-3}). A_{ki} is the transition probability between two energy levels. g_k is the degeneracy of the upper energy level. T is the plasma excitation temperature. E_k is the energy of the upper energy level. K_B is the Boltzmann constant. $U_S(T)$ is the partition function of element s at plasma excitation temperature T.

In a two-dimensional plane defined by x and y coordinates, each spectral line corresponds to a point. This plane is referred to as the Boltzmann plane. By performing a linear fit to the points representing spectral lines of the same element, the slope of the fitted line can be used to determine the plasma excitation temperature.

VI. Effect of Flow Velocity on LIBS Signal Intensity and LOD for Zn and Na.

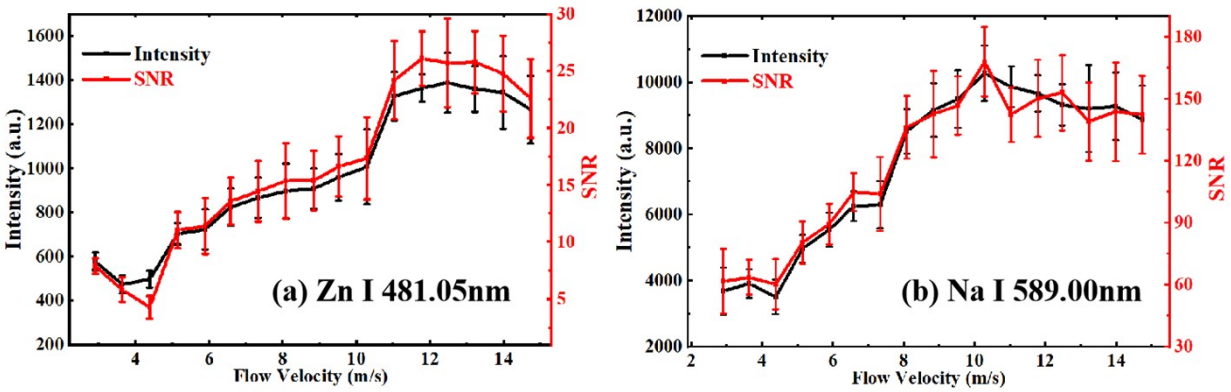

Fig. S4. The LIBS spectral intensities and SNRs at different flow velocities for (a) Zn I 481.05nm and (b) Na I 589.00nm.

To test the applicability of this method, we selected Zn and Na, which are commonly used as coolants in the nuclear industry. A 10000 mg/L standard zinc solution and a 1000 mg/L standard sodium solution were used as samples. Figure S4 shows the spectral intensity and signal-to-noise ratio (SNR) for Zn I 481.05 nm and Na I 589.00 nm at different flow velocities. It can be observed that the LIBS spectral intensity and SNR for both Zn and Na initially increase, then begin to decline at a critical flow velocity between 11.03 m/s and 14.73 m/s, exhibiting a trend similar to that shown in Figure 2 of the manuscript. Therefore, the approach of varying flow velocity to enhance LIBS signal intensity remains applicable for the detection of Zn and Na, demonstrating its overall applicability.

To evaluate the detection capabilities of this method for Zn and Na, calibration curves were constructed using standard zinc solutions at concentrations of 500, 1000, 2000, and 5000 mg/L, and standard sodium solutions at concentrations of 10, 20, 50, 100, and 200 mg/L. The limit of detection (LOD) was also calculated. Figure S5(a) presents the calibration curve for Zn at a flow velocity of 12.47 m/s, while Figure S5(b) shows the calibration curves for Na at flow velocities of 2.9 m/s and 12.47 m/s. Each data point in the figures was obtained by averaging 15 single measurements, with error bars representing the standard deviations. Table S4 lists the slopes of the calibration curves, the coefficients of determination (R^2), and the LOD.

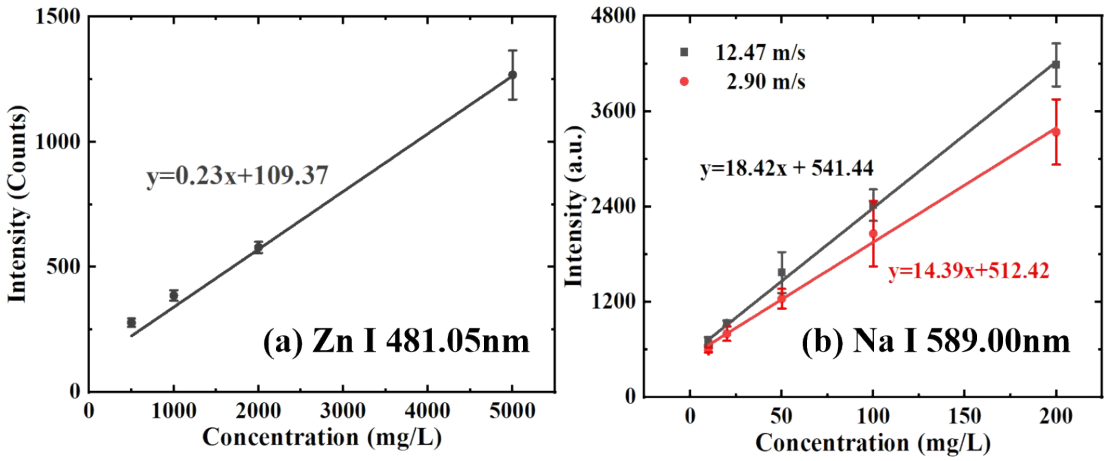

Fig. S5. The calibration curves of flow velocity at 12.47 m/s for (a) Zn I 481.05nm and (b) 2.9m/s and 12.47 m/s for Na I 589.00nm.

Table S4 The evaluation parameters of calibration curves.

Element	Flow velocity(m/s)	Slope	R^2	LOD(mg/L)
Zn I 481.05nm	12.47	0.23±0.01	0.9837	77.6
Na I 589.00nm	2.90	14.39±0.50	0.9952	1.24
Na I 589.00nm	12.47	18.42±0.64	0.9964	0.97

At a flow velocity of 12.47 m/s, the LOD for Zn is 77.6 mg/L. In contrast, at a flow velocity of 2.9 m/s, even a standard Zn solution at 5000 mg/L is difficult to detect. As for Na, the LOD is 1.24 mg/L at a flow velocity of 2.9 m/s, and this improves to 0.97 mg/L when the flow velocity is increased to 12.47 m/s.